Phenomenological description of the longitudinal vibrations of the quasi-one-dimensional solid PtCl: calculation of the valence defect frequencies

1991 J. Phys.: Condens. Matter 3 1709

(http://iopscience.iop.org/0953-8984/3/12/003)

J. Phys.: Condens. Matter 3 (1991) 1709–1726. Printed in the UK

Phenomenological description of the longitudinal vibrations of the quasi-one-dimensional solid PtCl: calculation of the valence defect frequencies

Alain Bulou†, Robert J Donohoe and Basil I Swanson
Inorganic and Structural Chemistry Group (INC-4), Isotope and Nuclear Chemistry Division, Los Alamos National Laboratory, Los Alamos, NM 87545, USA

Received 9 August 1990

Abstract. The longitudinal vibrations of the PtCl linear chain and those of various valence defects are described by a one-dimensional model in a first-nearest-neighbour interaction approximation. The analysis is performed as a function of the K_2/K_1 ratio (K_1 and K_2 representing the $PtCl^{IV}$–Cl and Pt^{II}–Cl force constants, respectively), which is shown to play an important role in the vibrational characteristics of the defects while the infrared frequencies are not strongly dependent on a particular ratio. A coherent description of the frequencies of the modes of the perfect chain and those of the polaronic defects is obtained for $K_2/K_1 = 0.3$. For this ratio the electron polaron and the electron bipolaron give rise to one Raman-active mode while at least two are predicted for the other investigated defects. The shapes of the Raman bands associated with the electron and hole polarons are explained by the chlorine isotopic effect. The vibration associated with the electron bipolaron is predicted to be at about 210 cm^{-1} where a broad line grows upon photolysis. An elementary calculation based upon a Born–Mayer potential for short-range interactions, adjusted from the interionic distances, leads to force constants of the same magnitude as those adjusted from the experimental frequencies.

1. Introduction

Halogen-bridged transition metal mixed-valence complexes (MX) have been studied extensively over the last decade as prototypical low-dimensional solids. The most widely studied system is $[Pt(en)_2][Pt(en)_2X_2](ClO_4)_4$ (where en ≡ ethylenediamine) referred to as PtX (X ≡ Cl, Br, I), and where changing the bridging halide from Cl to I changes the ground state from an extensively Peierls distorted strong charge-density wave (CDW) to a weak CDW structure with little distortion and charge separation [1–6]. Optical absorption [7, 8] and resonance Raman studies [9, 10] in combination with Peierls–Hubbard many-body calculations [11] have established the presence of local gap states (polarons and bipolarons) that arise from self-doping or photoexcitation [12, 13].

With the exception of the results of Degiorgi *et al* [14, 15], little work has been

† Permanent address: Laboratoire de Physique de l'Etat Condensé (Laboratoire associée au CNRS 807), Faculté des Sciences, Universite du Maine, 72017 Le Mans Cédex, France.

0953-8984/91/121709 + 18 $03.50

reported on the lattice dynamics of the different defects. Such a study should be helpful for the following reasons:

(i) to check the self-consistency of the proposed assignments for the defect Raman features;

(ii) to predict the number of effectively localized Raman-active modes for the various types of defect;

(iii) to explain the origin of the unassigned lines;

(iv) to predict the vibrational frequencies of the defects which have not yet been identified.

Such an approach should also be useful for comparison with more sophisticated descriptions such as the Peierls–Hubbard Hamiltonian from which such frequencies can also be deduced. In addition, the magnitude of the force constants for the normal chain and the defects can be a probe for the effective charge of the ions.

The present study is devoted to the strongly charge disproportionated PtCl which, up to now, has been the most extensively studied MX solid. This investigation concerns the longitudinal vibrations (which are more tightly coupled to the electronic properties) and is performed with a one-dimensional model in the first-nearest-neighbour interactions approximation. The role of second-nearest-neighbour interactions will also be examined (sections 3–10) in order to determine the extent to which the former approximation is valid. In the following, the experimental frequencies are expressed by their corresponding wavenumber in reciprocal centimetres.

2. Vibrations of the perfect chain

The PtCl structure has been described by Matsumoto *et al* [16] from single-crystal x-ray diffraction studies. At high temperatures it is orthorhombic† with cell parameters $a = 9.643$ Å, $b = 13.525$ Å and $c = 10.807$ Å. It mainly consists of linear $\ldots Pt^{II} \ldots Cl \ldots Pt^{IV} \ldots Cl \ldots$ chains along the c axis separated by ClO_4 counterions; the platinum ions are ligated equatorially by ethylenediamine. The interchain separation is large (8.38 Å) and, therefore, the Pt–Cl sublattice can be considered as a quasi-one-dimensional system. Such a schematization has already been used to describe the electronic properties [4–6, 11]. In this framework, the one-dimensional unit cell contains four atoms: Pt^{II}, Pt^{IV}, 2X (figure 1(*a*)). There are four phonon branches. For the wavevector $q = 0$, one mode is Raman active (ω_1), two are infrared active (ω_2 and ω_3 for high and low frequencies, respectively) and the fourth is the zero-frequency acoustic mode.

In a first-nearest-neighbours interaction model, the vibrations of the perfect chain are described by two force constants K_1 (Pt^{IV}–Cl interaction) and K_2 (Pt^{II}–Cl interaction) with K_2 smaller than K_1. The diagonalization of the 4×4 dynamical matrix for $q = 0$ leads to the following analytical expressions for the optically active modes:

$$\omega_1^2 = (K_1 + K_2)/m$$

$$\omega_2^2 = (K_1 + K_2)(1/M + 1/2m)(1 + \sqrt{1 - \alpha})$$

† It has been shown recently that PtCl undergoes a phase transition [17] and that, at the low temperatures at which the vibrational studies have been performed, is monoclinic. However, it can still be described in terms of chains and the interionic distances Pt–Cl are not significantly different from the published values.

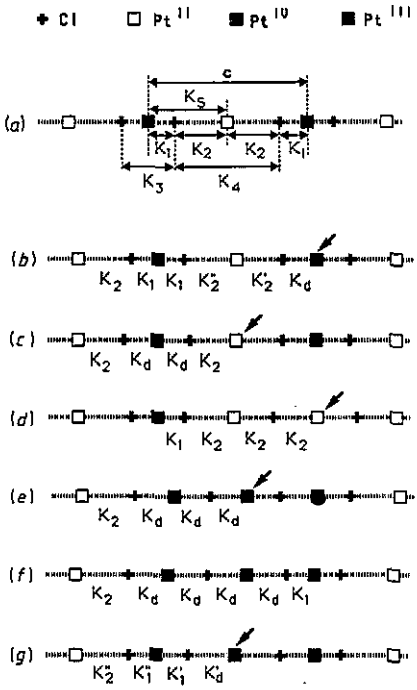

Figure 1. Schematization of (*a*) the perfect PtX chain and (*b*)–(*g*) the chain with the different kinds of defect studied: (*b*) electron polaron, (*c*) pair of electron polarons, (*d*) electron bipolaron, (*e*) exciton–electron polaron pair, (*f*) exciton and (*g*) hole polaron.

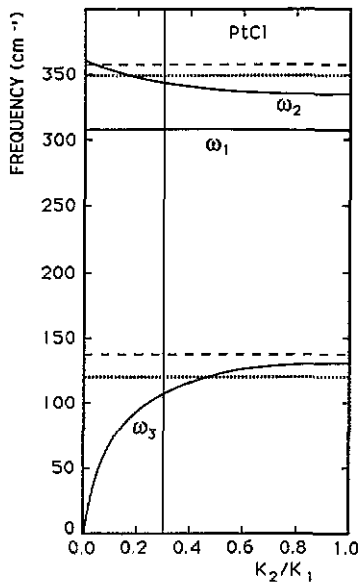

Figure 2. Calculated infrared frequencies ω_2 and ω_3 as functions of K_2/K_1 in the first-nearest-neighbour approximation. The Raman frequency ω_1 is kept equal to the experimental one (horizontal full line). The dotted and broken horizontal lines represent the experimental infrared frequencies according to [14] and [15], respectively. The vertical full line represents the value used to calculate the phonon spectrum (figure 4).

$$\omega_3^2 = (K_1 + K_2)(1/M + 1/2m)(1 - \sqrt{1 - \alpha})$$

where

$$\alpha = 16[K_1K_2/(K_1 + K_2)^2][m(M + m)/(M + 2m)^2]$$

and where M and m represent the metal and halogen masses, respectively. The sum $K_1 + K_2$ can be deduced from the Raman frequency which is unambiguously determined (308 cm^{-1})†: $K_1 + K_2 = 198.5$ N m^{-1} (= 1.985 mdyn $Å^{-1}$). In this first-nearest-neighbour interaction approach, the number of experimental data exceeds the number of parameters and the validity of the model can be checked. This is evidenced in figure 2 where the calculated frequencies ω_2 and ω_3 are plotted against the ratio K_2/K_1 keeping $K_1 + K_2$ (i.e. the Raman frequency) constant. The reported experimental infrared frequencies are 349 and 120 cm^{-1} [14] or 358 and 137 cm^{-1} [15]. A good description of the experimental values can be obtained for a wide range of K_2/K_1. Either of the reported frequencies for ω_2 would suggest K_2/K_1 close to zero (actually, the discrepancy with the

† The fine structure of this line [1, 18] is attributed to the relative disorder of the different chains [19].

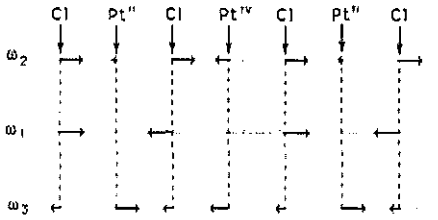

Figure 3. Normal coordinates of vibrations for the three optical modes of the perfect chain for $K_2/K_1 = 0.3$ in the first-nearest-neighbour interaction approximation.

experimental values is never greater than 7%) while ω_3 would indicate that this ratio is close to unity (such a result may partially explain why Degiorgi *et al* [14] and Clark *et al* [1] obtained different conclusions about the relative values of K_1 and K_2). As a consequence, the infrared frequencies cannot be used to obtain a reliable value of K_2/K_1 in the first-nearest-neighbour interaction approximation. On the other hand, this K_2/K_1 ratio is the key parameter for predicting the characteristics of the defect vibrations, even qualitatively. The approach used in this paper is to examine as a function of K_2/K_1 both the vibrational frequencies of the perfect chain and those of the defects in order to obtain a consistent set of force constants.

As will be shown, a coherent description of the vibrational properties of PtCl is obtained for K_2/K_1 close to 0.3 ($K_1 = 152.7\,\mathrm{N\,m^{-1}}$; $K_2 = 45.8\,\mathrm{N\,m^{-1}}$). The corresponding infrared mode frequencies of the chain are calculated at $343\,\mathrm{cm^{-1}}$ (2% or 4% difference from the experimental frequencies) and $108\,\mathrm{cm^{-1}}$ (10% or 21% differences from the experimental frequencies). The normal coordinates of the Brillouin zone centre optical modes are schematized in figure 3; note that for ω_3 the two platinum atoms move in opposite directions and that the frequency of this mode is sensitive to the second-nearest-neighbour force constant K_5 (see section 3.10). Using a model which includes transverse interactions, Degiorgi *et al* [14] proposed that $K_1 = 110\,\mathrm{N\,m^{-1}}$ and $K_2 = 87\,\mathrm{N\,m^{-1}}$ (i.e. $K_2/K_1 = 0.8$) which leads, in our description, to $\omega_1 = 307\,\mathrm{cm^{-1}}$, $\omega_2 = 334\,\mathrm{cm^{-1}}$ and $\omega_3 = 130\,\mathrm{cm^{-1}}$.

The calculated phonon spectrum for $K_2/K_1 = 0.3$ is represented by the full curves in figure 4 (the broken curves correspond to the second-nearest-neighbour approximation discussed in section 3.10). For K_2/K_1 close to zero the two high-frequency branches are flat while they collapse at the Brillouin zone boundary for $K_2/K_1 = 1$. In this latter case, no localized mode would be expected between the Raman and the high-frequency infrared modes. The frequency ranges where no local modes are predicted are represented by the shaded areas in figure 7; they correspond, for a given K_2/K_1 ratio, to the extent of the different dispersion branches.

3. Vibrations of the defects

3.1. Model

The frequencies and normal coordinates of vibration (along the chain) of the defects are obtained by solving the dynamical matrix for a chain consisting of 80 atoms (20 cells) or 82 atoms (for a kink, see section 3.9) including one defect or several defects and using cyclic boundary conditions [20]. Increasing the number of cells does not change the frequencies.

The interionic distances in PtCl are $d_1 = 2.318$ Å for Pt^{IV}–Cl and $d_2 = 3.085$ Å for Pt^{II}–Cl [16]. The creation of an electron bipolaron ($Pt^{IV} \rightarrow Pt^{II}$) requires a large increase

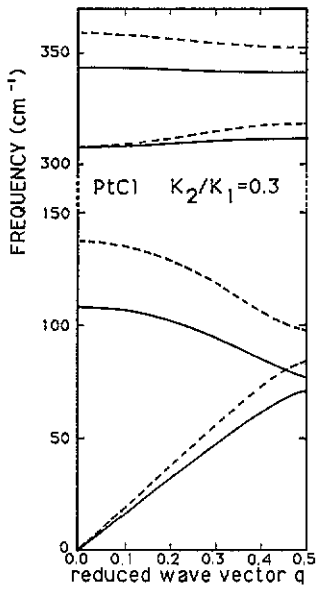

Figure 4. Calculated phonon dispersion curves, for $K_2/K_1 = 0.3$, in the framework of the first-nearest-neighbour interactions (———) and second-nearest-neighbour interactions for $K_3 = K_4$ (– – –). The reduced wavevector q is defined with respect to the reciprocal wavevector $c^* = 2\pi/c$, where c represents the cell parameter defined in figure 1.

in bond length, and the creation of a hole bipolaron ($Pt^{II} \rightarrow Pt^{IV}$) similarly requires a large decrease in bond length. On the other hand, it is more difficult to predict what happens during the creation of an electron or hole polaron since the Pt^{III}–Cl distance d_3 is not known. However, a simple description such as that used in the next section indicates that it should be intermediate between d_1 and d_2 and closer to d_1 than to d_2 ($d_3 = 2.66$ Å). Note also that in $K_4[Pt_2(P_2O_5H_2)_4Cl].3H_2O$, where the Pt^{III} ion exists, structural studies [21] give a Pt^{III}–Cl distance of 2.44 Å. Then it can be supposed that the less perturbing (photo)induced defect is the electron polaron; the Pt^{III}–Cl force constant deduced from the electron polaron frequency will be used in our model for most of the other defects although, when it is appropriate, some relaxations of the force constants have been included.

Most of the defects except the exciton (section 3.6) and the kink (section 3.9) exhibit a symmetry centre so that the modes can be classified into symmetric (Raman active) and antisymmetric (infrared active). However, the ^{35}Cl–^{37}Cl isotopic mixture is able to disturb significantly such a classification and can break the selection rules.

3.2. Electron polaron

As reported in [9, 10], the electron polaron Raman signature has been assigned to the 263 cm^{-1} feature (highest-frequency component) enhanced with the 1.29–1.44 and 1.97 eV excitation energies. As will be shown in the following, both the force constants required to describe such a frequency and the lineshape (related to isotopic effect) are consistent with this assignment. The schematization of the electron polaron is given in figure 1(*b*).

Assuming at first approach that the neighbouring force constants are not disturbed ($K_2'' = K_2' = K_2$), the Pt^{III}–Cl force constant K_d is uniquely deduced as a function of the K_2/K_1 ratio in order to fit a symmetric mode at 263 cm^{-1} (for a defect surrounded by the

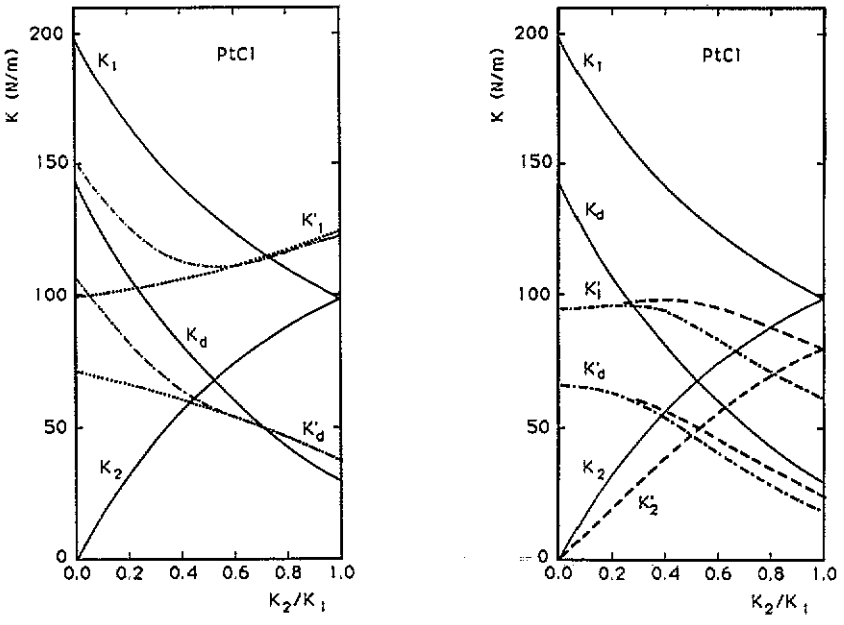

Figure 5. Evolution as a function of K_2/K_1 of the force constants required to describe the electron polaron frequency (———, K_d) and the hole polaron frequency in (*a*) case I and (*b*) case h for the three approximations B (. . . .), C (– · –) and D (– – –). The force constants K_1 and K_2 are drawn for comparison.

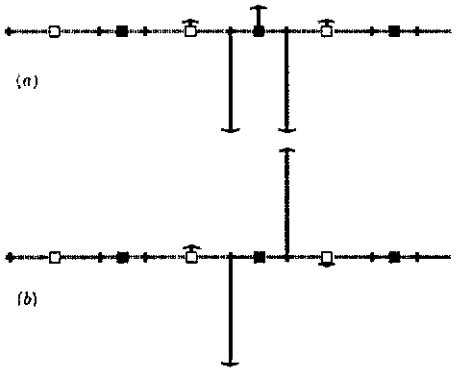

Figure 6. Schematization of the normal coordinates of vibration of the localized modes associated with an electron polaron (the ionic displacements are schematized normal to the chain for convenience): (*a*) antisymmetric mode; (*b*) symmetric mode.

^{35}Cl isotope). These K_d values are plotted in figure 5 together with K_1 and K_2 (full curves). The Pt^{III}–Cl force constant K_d is expected to be greater than K_2 (an additional positive contribution can also be expected owing to the 'stress' induced by the increase in the interionic distances concomitant with the creation of the electron polaron). As shown in figure 5, this condition is not fulfilled for K_2/K_1 greater than about 0.5. For $K_2/K_1 = 0.3$, the force constant K_d is close to $(K_2 + K_1)/2$. The ionic displacements that correspond to this localized mode are shown in figure 6(*b*) (for pure ^{35}Cl isotope). It appears that only the two chlorine atoms next to the defects undergo significant displacements and thus the vibrational frequency for this defect is mainly determined

by $K_2 + K_d$ which explains why this sum is almost constant irrespective of K_2/K_1 (figure 5). Another consequence of the localization is the fact that the isotopic mixture gives rise to only three lines corresponding to the three different configurations:

$$^{35}Cl\text{–}Pt^{III}\text{–}^{35}Cl: p = \tfrac{9}{16} \qquad \omega = 263\ cm^{-1}$$

$$^{35}Cl\text{–}Pt^{III}\text{–}^{37}Cl: p = \tfrac{6}{16} \qquad \omega = 259\ cm^{-1}$$

$$^{37}Cl\text{–}Pt^{III}\text{–}^{37}Cl: p = \tfrac{1}{16} \qquad \omega = 256\ cm^{-1}$$

where p represents the probabilities of each configuration and where the frequencies are calculated for $K_2/K_1 = 0.3$. This result is consistent with the shape of the experimental signal (figure 1 of [10] for 1.40 eV excitation).

No additional Raman-active mode is predicted for an electron polaron, but an infrared-active mode is expected at a frequency slightly higher than the defect-induced Raman frequency: from 306 cm^{-1} for $K_2/K_1 = 0$ to 265 cm^{-1} for $K_2/K_1 = 1$. The normal coordinates for this mode are drawn in figure 6(a). Owing to the isotopic mixture, the mode for a $^{35}Cl\text{–}Pt^{III}\text{–}^{37}Cl$ sequence, which is not purely antisymmetric, is expected to be slightly Raman active; this could possibly explain the signal enhanced for the same excitation energy as 263 cm^{-1}, in the frequency range 265–295 cm^{-1} (figure 1 of [10]); for $K_2/K_1 = 0.3$, the calculated frequency is 281 cm^{-1}.

As mentioned above, the creation of an electron polaron should be associated with an increase in the Pt–Cl distance, thus stressing the neighbouring bonds. As a result, the corresponding force constants K_2' and K_2'' (figure 1(b)) could be greater than the corresponding values in the perfect chain. Calculation shows that the modes are again strongly localized and the frequency is driven by $K_2' + K_d$; increasing K_2' roughly results in a decrease in K_d by the same amount (the same results are obtained whether $K_2'' = K_2$ or $K_2'' = K_2'$). Taking into account such an increase in K_2' does not change the isotopic effect but results in a slight decrease in the frequency of the infrared mode associated with the defect ($\Delta\omega = -0.46\ cm^{-1}$ for $\Delta K_2' = 1\ N\ m^{-1}$). No other change is predicted for $K_2'' = K_2$ but new localized modes are expected just above each of the dispersion branches for $K_2'' = K_2'$ provided that these values are greater than about 50 $N\ m^{-1}$. The frequencies of these new modes increase linearly with K_d'; for example for $K_d' = 76\ N\ m^{-1}$ and $K_2'' = K_2' = 62\ N\ m^{-1}$, symmetric and antisymmetric modes are predicted at 348 cm^{-1} and 315 cm^{-1} and an antisymmetric mode is predicted at 112 cm^{-1}. Actually, as suggested from the study of the electron bipolaron (see below), the increase in the interionic distance can probably be satisfied by pushing the chlorine atoms off the chain axis and then the Pt^{II}–Cl distance next to the defect and K_2' should not be significantly changed with respect to their values in the perfect chain.

3.3. Pair of electron polarons

These kinds of defect are schematized in figure 1(c). According to the earlier electronic calculations using a Peierls–Hubbard Hamiltonian [11], they are unstable with respect to the electron bipolaron. However, they could be stabilized for a slightly different set of parameters and their frequency should be estimated.

These defects should be characterized by the same force constant as the electron polaron and their vibrational frequencies should be close to those calculated using K_d.

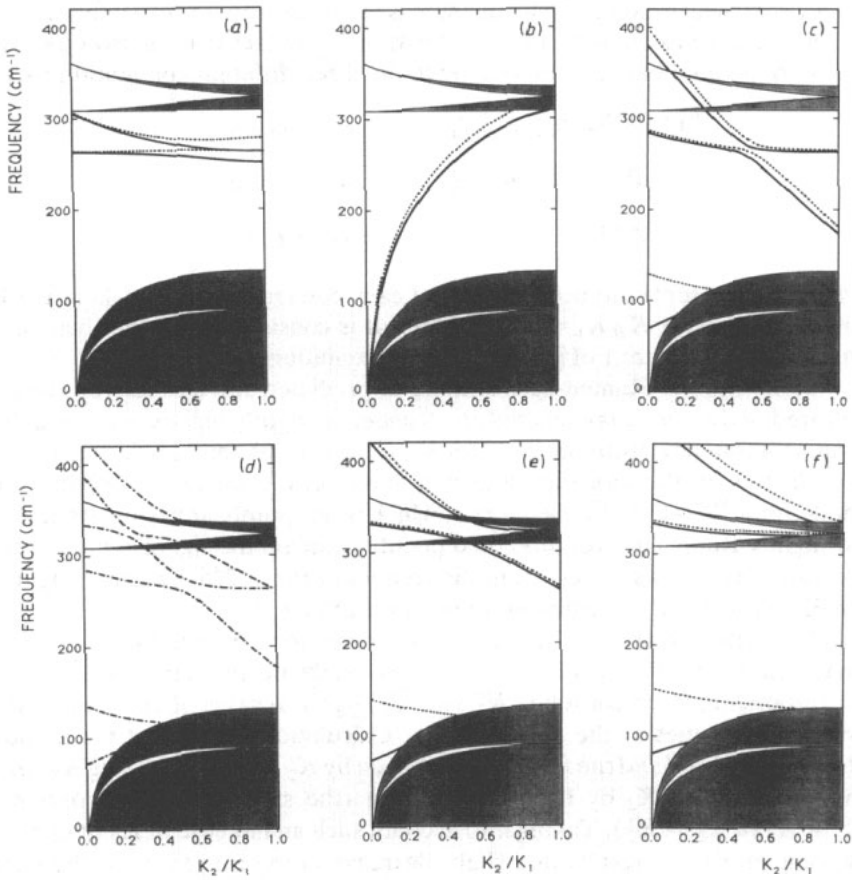

Figure 7. Calculated frequencies of the localized modes associated with the selected defects ((*a*) pair of electron polarons, (*b*) electron bipolaron, (*c*) exciton–electron polaron pair, (*d*) exciton, (*e*) 'free-chain' hole polaron and (*f*) 'free-chain' hole bipolaron) for ^{35}Cl components: ———, symmetric modes; . . . , antisymmetric modes; – · –, non-symmetric modes; ■, region where no localized mode is allowed.

They are plotted in figure 7(*a*) as a function of K_2/K_1 for pure ^{35}Cl components. Two Raman-active modes are expected. The ionic displacements for the purely symmetric modes (^{35}Cl) for $K_2/K_1 = 0.3$ are similar to those represented in figure 10 (with respect to the symmetry centre) except that the relative amplitude of vibration of the two kinds of chlorine atom are reversed. It appears that four chlorine atoms are involved and, as a result, the isotopic mixture leads to ten combinations (table 1) and to a multicomponent Raman signal as represented in figure 8 for $K_2/K_1 = 0.3$. Such defects (if any) could contribute to the Raman intensity observed in this frequency range where a mode associated with the hole polaron mode is also located [10].

3.4. Electron bipolaron

According to the electronic calculations [11], this kind of defect is predicted to be stable and, in PtCl, it should be enhanced with 1.75 eV excitation energy [11]. This energy

Table 1. Probabilities of the ten ^{35}Cl and ^{37}Cl combinations of four chlorines. Asterisks denote the combinations that do not lead to purely symmetric and antisymmetric modes.

Combination	Probability (×1/256)
35–35–35–35	81
35–35–35–37	54*
35–35–37–35	54*
35–35–37–37	18*
35–37–35–37	18*
35–37–37–35	9
37–35–35–37	9
35–37–37–37	6*
37–35–37–37	6*
37–37–37–37	1

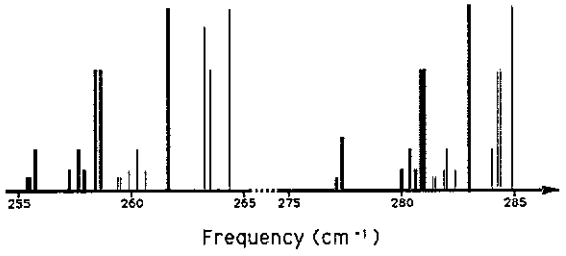

Figure 8. Isotopic effect: relative contributions of the different modes associated with a pair of electron polarons (for $K_2/K_1 = 0.3$): I, purely symmetric modes; I, purely antisymmetric modes; ≡ modes which are not strictly symmetric; ⋮, modes which are not strictly antisymmetric.

range has never been investigated and, up to now, no vibrational signature for the electron bipolaron has been reported. On the other hand, the frequencies associated with this defect can be estimated since, in the simplest approximation, it depends only on the Pt^{II}–Cl force constant, i.e. the force constant K_2 of the perfect chain (figure 1(*d*)). The frequencies of the modes associated with the electron bipolaron are plotted in figure 7(*b*) (full curve for the symmetric mode) as a function of K_2/K_1 for the ^{35}Cl components. These frequencies vary extensively and for $K_2/K_1 = 0.3$ the Raman-active value is about 210 cm^{-1}. As seen in figure 1 of [9] (for 1.65 eV excitation), a broad signal appears in this frequency range after photolysis and, since the 215 cm^{-1} line, which is characteristic of the N–Pt–N vibration [22], no longer emerges from the background, it is likely that the broad feature at 210 cm^{-1} is photoinduced. We attribute this photoinduced band to an electron bipolaron. An additional reason to believe such an assignment arises from the fact that similar analysis performed on the isomorphous PtBr also predicts for the electron bipolaron a frequency where an intense and (again) broad line is observed upon photolysis [23].

The normal coordinates of vibration of the symmetric mode for $K_2/K_1 = 0.3$ are very close to those of the electron polaron represented in figure 6 (with respect to the symmetry centre) and so, again, only the Cl ions next to the Pt^{II} defect undergo significant

displacements. Consistently, the isotopic effect leads to three components with the following frequencies for $K_2/K_1 = 0.3$:

$$^{35}Cl\text{–}Pt^{III}\text{–}^{35}Cl: p = \tfrac{9}{16} \qquad \omega = 215.8\ cm^{-1}$$

$$^{35}Cl\text{–}Pt^{III}\text{–}^{37}Cl: p = \tfrac{6}{16} \qquad \omega = 212.2\ cm^{-1}$$

$$^{37}Cl\text{–}Pt^{III}\text{–}^{37}Cl: p = \tfrac{1}{16} \qquad \omega = 210.2\ cm^{-1}.$$

As mentioned above, the creation of an electron bipolaron should be associated with increases in the bond lengths and the force constants surrounding the defect; in the absence of the exact frequency such force constants cannot be determined in detail but it has been checked that this should not cause any qualitative change. On the other hand, such as increase in interionic distances can be satisfied by pushing the chlorine atoms out of the chain, which could explain the width of the line [9]; the different chlorine atoms can experience different force fields according to their position with respect to the neighbouring ClO_4^- which, for the normal chain, are predicted to give a contribution of about 10 N m^{-1} [19]. Under such a hypothesis, using the distances d_1 and d_2, the Pt–Cl bond is estimated to be about 17° from the chain axis. This could also induce some Raman activity into the antisymmetric mode which is predicted at a slightly higher frequency (figure 7(*b*)), thus giving an extra contribution to the broadening (in addition to that due to isotopic mixing). Of course, to confirm this assignment it would be desirable to study the system with 1.75 eV energy where the electron bipolaron is expected to be enhanced.

3.5. Exciton–electron polaron pair

The pinning of an exciton by a pre-existing electron polaron to form an exciton–electron polaron pair is schematized in figure 1(*e*). Although this structure has never been previously considered, we would like to present some results about this defect for several reasons. Such a defect is expected to be weakly perturbing; using the d_3-value estimated in section 3.1, such a defect should lead to an increase of 0.07 Å per bond instead of the 0.33 Å increase associated with the creation of an electron polaron. It must also be noted that such a defect can be created next to an electron polaron without the appearance of the asymmetric configuration of an exciton (and this may be the driving force for exciton pinning):

$$\ldots 4242324 \ldots \rightarrow \ldots 4233324 \ldots$$

Since it is associated with a (small) increase in bond length, like the electron polaron, the force constant required to calculate its frequency should not be significantly different from those adjusted from the electron polaron frequency. The frequencies associated with this defect are plotted in figure 7(*c*) as a function of K_2/K_1. It appears that this kind of defect should give rise to two Raman-active modes, predicted to be at 272.7 and 323.2 cm^{-1} for $K_2/K_1 = 0.3$ (^{35}Cl components). Indeed, as shown in figure 1 of [10], for the 1.83 eV excitation energy, the (unassigned) 272 cm^{-1} line is enhanced at the same time as a line in the vicinity of 320 cm^{-1}. The normal coordinates for these modes look roughly like those represented later in figure 10 (with respect to the symmetry centre) with, however, a greater difference between the relative amplitudes of motion of chlorine atoms. The four chlorine atoms are significantly involved in such vibrations and again

the isotopic mixture leads to several lines (table 1). However, for $K_2/K_1 = 0.3$, most of these lines are superimposed and only two bands are predicted.

3.6. Exciton

The vibrational signatures of the exciton have never been reported and an estimation of the frequencies could help to identify them in time-resolved resonance Raman studies. It can be thought that the perturbation induced by the creation of such a defect is weak (figure 1(*f*)) since the increase in bond length required by the transformation $Pt^{IV} \rightarrow Pt^{III}$ is compensated by the decrease required by the neighbouring transformation $Pt^{II} \rightarrow Pt^{III}$ (using the estimated value of d_3 the total change in bond length is -0.04 Å per bond). Then, the force constant K_d deduced from the electron polaron frequency could give a reasonable value of the frequencies associated with the exciton. As shown in figure 7(*d*), four lines are expected and, because of the lack of symmetry centre (figure 1(*f*)), none of them is purely symmetric or antisymmetric. The two resonance Raman modes enhanced at 1.85 eV (see section 3.5) could also be attributed to the exciton, although the expected high-frequency components are not observed.

3.7. 'Free-chain' hole polaron and hole bipolaron

As will be shown in section 4, the creation of a hole polaron or a hole bipolaron requires a significant decrease in bond length and the force constants next to the defect can be smaller than those deduced from the perfect chain or the electron polaron. However, the system may contain similar pre-existing defects (which, like the photoinduced defects, can give rise to a significant intensity due to resonance enhancement) and the interionic distance around such pre-existing hole polarons or hole bipolarons may not be stressed as expected for the photoinduced ones. Moreover, up to now there has been no experimental evidence for the fact that the chains are too strongly connected to the rest of the crystal to prevent the Pt^{III}–Cl and Pt^{IV}–Cl distances in the neighbourhood of the holes from having the values that they would have in 'free' chains, i.e. relaxed chains. Thus, we have to consider the frequencies of the modes associated with these polarons such that $K'_d = K_d$, $K''_1 = K'_1 = K_1$ and $K''_2 = K_2$ (figure 1(*g*)). They are plotted in figures 7(*e*) and 7(*f*) for the hole polaron and hole bipolaron, respectively. For K_2/K_1 less than 0.5, two Raman-active modes are expected above the 308 cm^{-1} mode of the normal chain. Such defects can reasonably explain the unassigned high-frequency lines enhanced at high energy (above 2.18 eV in figure 1 of [10]). However, in the absence of additional experimental confirmation a detailed assignment would be hazardous.

3.8. 'Pinned' hole polaron

According to [9, 10], the 287 cm^{-1} band, enhanced with 1.65 eV excitation, is the signature of the photoinduced hole polaron since, upon photolysis, this line grows at the same rate as the 263 cm^{-1} electron polaron band and since such features can be correlated with the photoinduced A, B and C bands that have been attributed to polarons. Such an assignment is also consistent with the electronic calculations [11]. The Raman signal exhibits a three-component shape (curve resolution leads to at least five lines [10]); in the following, the highest-frequency component of this band (291 cm^{-1}) will be considered as the mode associated with the vibrations of ^{35}Cl although the 287 cm^{-1} line is more intense and exhibits overtones.

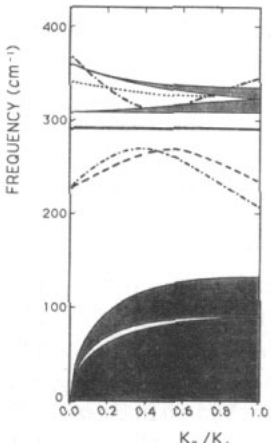

Figure 9. Calculated frequencies of the localized modes associated with the pinned hole polaron in case l (above 291 cm^{-1}) and in case h (below 291 cm^{-1}) in approximations B, C and D: symbols as in figure 5.

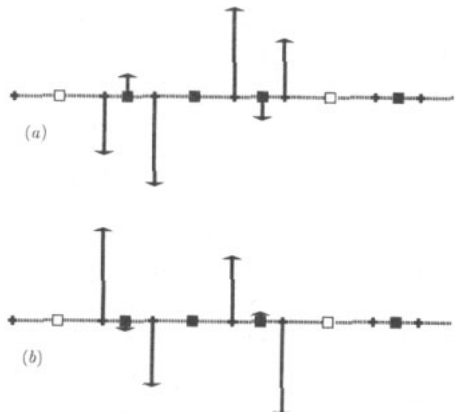

Figure 10. Schematization of the symmetric normal coordinates of vibration of the localized modes associated with a 'pinned' hole polaron for case h in approximation C ($K_2/K_1 = 0.3$ and ^{35}Cl isotope): (*a*) high-frequency mode; (*b*) low-frequency mode. The ionic displacements are schematized normal to the chain for convenience.

The force constants required to describe such a hole polaron are represented in figure 1(*g*). As mentioned above, in the absence of relaxation, the Pt^{III}–Cl bond length for a photoinduced hole polaron ($Pt^{II} \rightarrow Pt^{III}$) should be longer than that of a 'free' Pt^{III}–Cl and the corresponding force constant K_d' is expected to be smaller than that calculated, for example, for the electron polaron. The neighbouring Pt–Cl bond lengths can themselves be expanded and the associated force constants may also decrease. In order to determine at least the qualitative behaviour, the dynamical properties associated with this kind of polaron are calculated in several approximations: corrections limited to K_d' (case A), K_d' and K_1' (case B), K_d', K_1' and K_1'' (case C) and K_d', K_1', K_1'' and K_2'' (case D). It has also been assumed that the relative decrease with respect to the unperturbed force constants does not depend on the bond ($R = K_i'/K_i = K_i''/K_i$). This is obviously a very rough approximation since closer to the defect the force constants are affected significantly. So for cases C and D the K_d'-values are probably overestimated while the K_1'-values are underestimated; the (more realistic) intermediate cases can be estimated from these limiting approximations. As shown below, two modes are predicted to be Raman active so that two cases must be considered whether the 291 cm^{-1} line corresponds to the low-frequency mode (case l) or to the high-frequency mode (case h).

The force constants required in case l are plotted in figure 5(*a*). For case A, K_d increases roughly linearly from 0 N m^{-1} for $K_2/K_1 = 0.25$ to 70 N m^{-1} for $K_2/K_1 = 1$; there is no solution for $K_2/K_1 < 0.25$. The force constants for case D are very close to those for case C (much closer than in case h represented in figure 5(*b*)). For $K_2/K_1 \geqslant 0.7$, both approximation C and approximation D require the unrealistic condition $K_1' > K_1$. The calculated Raman-active frequencies are plotted in figure 9 and the normal coordinates of vibrations, for $K_2/K_1 = 0.3$, are similar to those schematized in figure 10. In all cases, two infrared-active modes are predicted with frequencies slightly higher (within the 10 cm^{-1} range) than the Raman values.

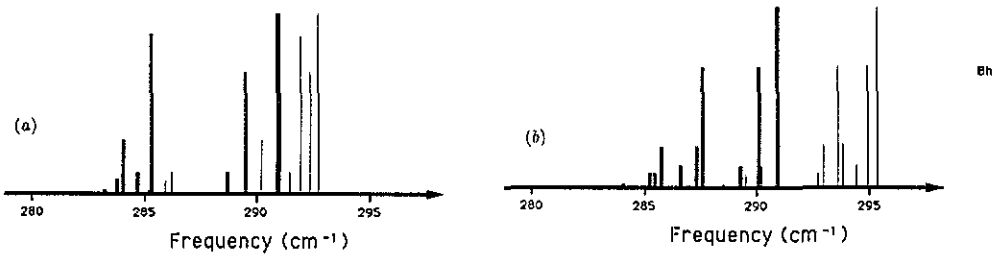

Figure 11. Isotopic effect: relative contributions of the different modes associated with a 'pinned' hole polaron (for $K_2/K_1 = 0.3$) in approximation C for (*a*) case l and (*b*) case h: symbols as in figure 8.

The force constants required to match the high-frequency Raman mode with the 291 cm^{-1} band are plotted in figure 5(*b*). There is no solution for cases A and B. As in case l, approximations C and D lead to similar values of the force constants. The Raman frequencies are plotted in figure 9 and the normal coordinates (^{35}Cl, symmetric modes) are schematized in figure 10 for $K_2/K_1 = 0.3$. As in case l, infrared modes are predicted at a frequency slightly higher than the Raman modes.

The isotopic effect on the 291 cm^{-1} line is schematized in figure 11 for $K_2/K_1 = 0.3$. Both case l and case h can reasonably explain the frequency extent of the experimental Raman signal as a consequence of the isotopic mixture; since an 'antisymmetric' mode appears in the same frequency range, the 'Raman band' can be made of up to 16 lines (table 1). It can be noted that the experimental shape [10] is even very close to that corresponding to the case h situation if one assume that the highest-frequency 'Raman component' is the 287 cm^{-1} line; the (broad) 291 cm^{-1} band would be due to (several) Raman-activated 'infrared modes'. Such a qualitative difference between the 287 cm^{-1} line and the 291 cm^{-1} line could explain why the former exhibits an overtone while the latter does not [10]. The force constants derived for this particular assignment are $K_d' = 57.5\ N\ m^{-1}$ and $K_l' = 93.1\ N\ m^{-1}$. However, considering the approximations, this interpretation must be considered to be tentative and it would be useful to perform experiments on pure $Pt^{35}Cl$ as a check.

The important result from these calculations is that, irrespective of the approximation, two Raman-active modes are predicted to be associated with the hole polaron. Up to now, only one has been experimentally reported. In case l, the second mode could be under or just above the (intense) ν_1 band of the perfect chain; the presence of a signal in the vicinity of 320 cm^{-1} at 1.65 eV, although not definite, cannot be excluded (figure 1 of [10]). In any case, in both case l and case h, the 'missing' mode may have a very weak intensity. A search for this mode would be useful in order to estimate the Raman polarizability tensor component associated with the three different kinds of bond (Pt^{II}–Cl, Pt^{III}–Cl and Pt^{IV}–Cl) and then to predict the intensities associated with other types of defect (provided that similar electronic couplings exist).

An estimation of the vibrational characteristics associated with the 'pinned' hole bipolaron can be deduced from the above force constants. In this case, as a first approach, only K_l' is required. The corresponding frequencies are plotted in figure 12 using K_l' as deduced from cases l and h in approximation C. The two cases lead to the prediction of two Raman-active modes (a third is predicted just above the low-frequency infrared mode for small values of K_2/K_1). We note that in case h, for $K_2/K_1 = 0.3$, the two modes

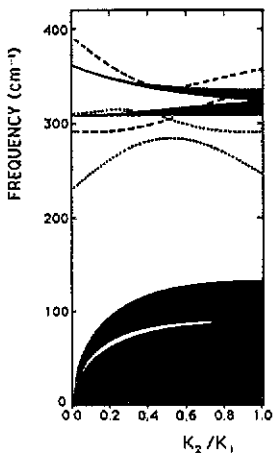

Figure 12. Estimation in approximation C of the frequencies of the localized modes associated with the 'pinned' hole bipolaron in case l (– – –) and in case h (· · · ·)).

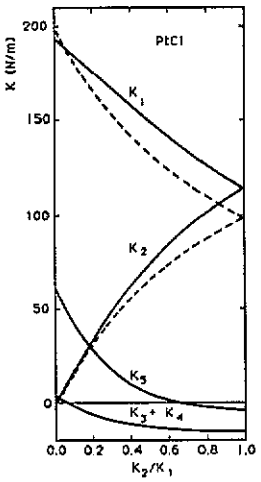

Figure 13. Evolution, as a function of K_2/K_1, of the force constants required to fit the Raman and infrared frequencies in a second-nearest-neighbour interaction approximation (——): – – –, corresponding force constants in the first-nearest-neighbour approximation.

are predicted at about 314 and 274 cm^{-1}; this provides an alternative explanation for the unassigned lines discussed in sections 3.5 and 3.6.

3.9. Charged kink '234'

One of the simplest defects proposed to explain the existence of a photoinduced EPR signal [24] is the (non-symmetric) charged kink '234', i.e. the sequence

$$\ldots X \ldots Pt^{IV} \ldots X \ldots Pt^{II} \ldots X \ldots Pt^{III} \ldots X \ldots Pt^{IV} \ldots X \ldots Pt^{II} \ldots .$$

The estimation of the force constants required to describe the dynamical properties of a kink is hazardous since the creation of such a defect must be associated with an important structural rearrangement and thus the systematic investigations will not be discussed in this article. It is, however, worth noting that, using the force constants K_1, K_2 and K_d adjusted from the electron polaron frequency, four modes are predicted at 367 cm^{-1}, 323 cm^{-1}, 273 cm^{-1} and 115 cm^{-1} (for the ^{35}Cl isotope). The second and third modes (which are only weakly dependent on K_2/K_1 if less than 0.5) can explain the unassigned lines enhanced at 1.83 eV previously discussed in section 3.5. These modes involve mainly one chlorine atom and so the isotopic effect roughly consists of two components with relative intensities 3:1 (the lines associated with the ^{37}Cl isotope are calculated at 267 and 316 cm^{-1}). Such an assignment is reasonable since the 272 cm^{-1} line and the EPR signal have similar qualitative behaviours; they both disappear above about 200 K [24].

3.10. Concluding remarks

In all cases, the defect vibrations have been found to be fairly localized and it has been checked that two defects cannot interact (to give rise to new modes) unless they are very

close together; all the calculations have been performed on a single defect or adjacent defects. No strongly resonant mode has been noted but less localized modes are predicted in the narrow low-frequency gap for several defects (electron bipolaron, exciton + electron polaron, etc).

As evidenced for several cases in figure 7, the localized modes may disappear into the phonon bands for some K_2/K_1 values, and so in the neighbourhood of such values the qualitative behaviour could be changed under the effect of any (neglected) extra interaction. This is especially true in the vicinity of the infrared frequencies which are not exactly described by the present model.

As will be shown in a forthcoming article [19], in addition to the first-nearest-neighbour Pt–Cl interactions, the only significant interactions (between the ions of the chain) are due to first-nearest-neighbour Pt–Pt electrical interactions (strongly charged ions) and, to a lesser extent, to Cl–Cl interactions. Such interactions can be taken into account by a model which includes second-nearest-neighbour force constants K_3, K_4 and K_5 (figure 1(a)). These force constants calculated using the Raman and infrared frequencies [15] are represented in figure 13. It appears that the K_1 and K_2 values are not strongly changed and that reasonably small values of the second-nearest-neighbour force constants (and smaller than K_1 and K_2 for $K_2/K_1 \geqslant 0.2$) can account for the discrepancy between the experimental infrared frequencies and the calculated values in the first-nearest-neighbour interaction approximation; it can be thought that, in addition to the contribution of the 'transverse bonds' taken into account by Degiorgi *et al* [14], the discrepancies mainly arise from neglecting K_5 (which, using the approach presented in section 4, should be positive and smaller than about 23 N m^{-1}). The dispersion curves calculated in the second-nearest-neighbour approximation for $K_2/K_1 = 0.3$ are shown (broken curves) in figure 4. The correction mainly consists of a shift of the 'infrared branches'. Most of the Raman-active modes associated with the defects do not involve significant displacements of platinum and do not depend strongly on K_5; their frequencies are probably more accurately described in the first-nearest-neighbour approximation than those of the infrared modes.

4. Estimation of the d_3 distance and of the force constants

The chains are made up of two kinds of platinum and two distances (d_1, Pt^{IV}–Cl; d_2, Pt^{II}–Cl) are crystallographically observed [16]. In an ionic description (PtCl is expected to be one of the more ionic compounds of the series), the system can be described in terms of electrical interactions and short-range repulsive interactions that can be represented by a Born–Mayer potential $A \exp(-r/\rho)$ (where r is the interionic distance, and A and ρ are parameters characterizing the potential). For interaction of two ions, the electrical contribution depends on the ionic charges while the short-range contribution depends on A and ρ, which can be adjusted from the two distances d_1 and d_2. Because of their distances, the neighbouring chains do not play a significant role while the ClO_4^- counterions give similar contributions to both bonds. In a first-nearest-neighbour interaction approximation, using +4, +2 and −1 for Pt^{IV}, Pt^{II} and Cl^-, respectively, the parameter ρ is found to be equal to 0.606 Å, which leads to $d_3 = 2.66$ Å for the Pt^{III}–Cl distance; taking into account the ions of the chain which are further removed and neglecting any screening effects lead to a slightly higher value.

The above description also makes it possible to calculate the force constants themselves which are primarily due to first-nearest-neighbour interactions. The calculated

values of K_1 and K_2 are 135 N m^{-1} and 48 N m^{-1}, respectively, so that $K_1 + K_2 =$ 183 N m^{-1}, a value (surprisingly) in good agreement with the magnitude calculated from the Raman frequency, 198 N m^{-1} (an extra contribution from ClO_4 is also expected); note that K_2 is much smaller than K_1. The predicted value for K_d is 89 N m^{-1}, i.e. intermediate between K_1 and K_2, in agreement with the adjusted values for $K_2/K_1 =$ 0.3. In the same way, for a hole polaron, in approximation B, the Pt^{IV}–Cl and Pt^{II}–Cl are calculated at $d_1' = 2.47$ Å and $d_3' = 2.93$ Å, leading to force constants of 98 N m^{-1} and 48 N m^{-1}, respectively; the large decrease in the adjusted force constants K_1' and K_d' required to describe the hole polaron frequency is not inconsistent with the predictions of the above model. It must be noted that the force constants calculated in the above approach decrease significantly as the effective charges decrease; for PtCl, the platinum charges must be close to +4 and +2 to get agreement with the experimental values while, for PtBr and PtI, smaller effective charges are required. A detailed analysis in the framework of the above description could give valuable information about the effective ionic charges together with the prediction of the force constants associated with the defects.

As shown in section 2, the infrared frequencies are not strongly dependent on K_2/K_1. On the other hand, the description of the electron polaron frequency requires $K_2/K_1 < 0.5$, and $K_2/K_1 = 0.3$ leads to K_d close to $(K_1 + K_2)/2$. For such a ratio, the electron bipolaron is expected to give a mode at a frequency where a photoinduced line is indeed observed; in a first-nearest-neighbour interaction model, a K_2/K_1 ratio close to 0.3 gives a coherent description of the vibrational frequencies. All the force constants (including those associated with the 'pinned' hole polaron) are of the same magnitude as those deduced from the simple description in the framework of a Born–Mayer potential, adjusted from the interionic Pt–Cl distances. Although encouraging, this latter description must be considered carefully since it is strongly dependent on the effective ionic charges.

5. Conclusion

In this paper, it has been shown that in a first-nearest-neighbour interaction approximation a coherent description of the frequencies of vibration of both the defects and the perfect PtCl chain can be obtained for K_2/K_1 close to 0.3 while $K_2/K_1 = 0.8$ was previously proposed based upon infrared frequencies [14, 15]; we have shown that in such an approach the calculated infrared frequencies are not strongly dependent on K_2/K_1 and that, on the other hand, their description may require one to take into account second-nearest-neighbour force constants.

Only one Raman-active mode is predicted to be associated with the electron polaron and the experimental shape can be explained by the chlorine isotopic mixture. The force constant K_d required to obtain this frequency is (as physically expected) less than K_2 provided that $K_2/K_1 \leqslant 0.5$.

Two Raman-active modes are predicted to be associated with the hole polaron while only one band has been experimentally reported, at about 287 cm^{-1}. It has been shown that the modes associated with this defect involve motions of four chlorine atoms so that the isotopic mixture can lead to a Raman band made of up to 16 lines since 'pseudo-antisymmetric' modes occur in the same frequency range. This can explain the structure of the experimental signal whose shape is consistent with the calculated shape in the case

where the 287 cm^{-1} band would correspond to the high-frequency component. The reason why the lower-frequency component is not seen remains unexplained.

The frequencies associated with several other defects have been calculated on the basis of the force constants deduced from the electron and hole polarons. For the electron bipolaron, a mode is predicted in the vicinity of 210 cm^{-1} where a broad line grows upon photolysis. We think that the broad character of this line may be due to displacement of the chlorine atoms from the chain axis in order to relax the stress caused by the increased bond length associated with the creation of such a defect. Four defects—the exciton, the exciton–electron polaron pair, the 'pinned' hole bipolaron and the charged kink—give rise to a Raman-active mode in the vicinity of 272 cm^{-1} where an unassigned line has been reported.

From these results, it would be interesting to check whether the line attributed to the electron bipolaron is enhanced at the energy predicted from the electronic band-structure calculation; this energy range has never been investigated. Detailed characterization of this mode would be interesting since its frequency is quite sensitive to the value of K_2/K_1.

The isotopic mixture has been useful to characterize defect lines since it reveals the number of chlorine atoms involved in the vibration. Experimental investigations on isotopically pure $Pt^{35}Cl$ would be interesting in order to resolve the multiple features which extend from about 263 to 295 cm^{-1}, and especially to check whether the 287 cm^{-1} band loses its structure and whether the 291 cm^{-1} component is due to an 'antisymmetric' mode activated by isotopic disorder; the better resolution and the greater intensity should help the search for the additional missing mode associated with the 'pinned' hole polaron.

It has been shown that the infrared frequencies are not strongly sensitive to the K_2/K_1 ratio. On the other hand, the Brillouin zone boundary frequencies are very sensitive to such a ratio; the experimental investigation of the phonon spectrum by inelastic neutron scattering would be useful to obtain a better estimation of K_2/K_1. This is also of interest since, according to our preliminary calculations, the force constants could be used to probe the effective ionic charges; this could be obtained from the description of the phonon dispersion curves with a rigid-ion model.

PtCl has been the most widely studied compound so that it can be considered as a reference system. However, many other materials are currently being studied in order to examine systems with intermediate-strength CDW character. The diagrams giving the defect frequencies as a function of the dimensionless K_2/K_1-ratio for PtCl are expected to be a qualitative guide to the first investigations of the defect vibrations in these new systems.

Acknowledgments

The authors would like to thank C T Arrington for helpful discussions. This work was performed under the auspices of the US Department of Energy with support from Material Science Division of the OBES and the Center for Material Science at Los Alamos National Laboratory. One of us (AB) is grateful for the receipt of a CNRS–National Science Foundation grant.

References

[1] Clark R J H 1984 *Advances in Infrared and Raman Spectroscopy* vol II, ed R J H Clark and R E Hester (New York: Wiley), pp 95–132, and references therein

[2] Ueta M, Kanzaki H, Kobayashi K, Toyazawa Y and Hanamura E 1986 *Excitonic Processes in Solids (Springer Series in Solid State Sciences 60)* (Berlin: Springer)
[3] Onodera Y J 1987 *J. Phys. Soc. Japan* **56** 250–9
[4] Nasu K and Mishima A 1988 *Rev. Solid State Sci.* **2** 539
[5] Baeriswyl D and Bishop A R 1988 *J. Phys. C: Solid State Phys.* **21** 339–56
[6] Conradson S D, Stroud M A, Zietlow M H, Swanson B I, Baeriswyl D and Bishop A R 1988 *Solid State Commun.* **65** 723–9
[7] Kurita S and Haruki M 1989 *Synth. Met.* **29** F129–36
[8] Donohoe R J, Ekberg S A, Tait C D and Swanson B I 1989 *Solid State Commun.* **71** 49–52
[9] Donohoe R J, Dyer R B and Swanson B I 1990 *Solid State Commun.* **73** 521–5
[10] Donohoe R J, Tait C D and Swanson B I 1990 *Chem. Mater.* **2** 315–9
[11] Gammel J T, Donohoe R J, Bishop A R and Swanson B I 1990 *Phys. Rev.* B **42** 10566–8
[12] Kurita S, Haruki M and Miyagawa K 1988 *J. Phys. Soc. Japan* **57** 1789–96
[13] Matsushita N, Norimichi K, Ban T and Tsujikawa I J 1987 *J. Phys. Soc. Japan* **56** 3808–11
[14] Degiorgi L, Wachter P, Haruki M and Kurita S 1989 *Phys. Rev.* B **40** 3285–93
[15] Degiorgi L, Wachter P, Haruki M and Kurita S 1990 private communication; 1990 *Phys. Rev.* submitted
[16] Matsumoto N, Yamashita M, Ueda I and Kida S 1978 *Mem. Fac. Sci. Kyushu Univ.* C **11** 209–16
[17] Huckett S C, Donohoe R J, Worl L A, Bulou A, Burns C and Swanson B I 1990 *Chem. Mater.* at press
[18] Tanaka M and Kurita S 1986 *J. Phys. C: Solid State Phys.* **19** 3019–28
[19] Bulou A, Donohoe R J and Swanson B I 1991 unpublished
[20] Barker A S Jr and Sievers A J 1975 *Rev. Mod. Phys.* **47** S1–79
[21] Butler L G, Zietlow M H, Che C M, Schaefer W P, Sridhar S, Grunthaner P J, Swanson B I, Clark R J H and Gray H B 1988 *J. Am. Chem. Soc.* **110** 1155–62
[22] Campbell J R, Clark R J H and Turtle P C 1978 *Inorg. Chem.* **17** 3622–8
[23] Bulou A, Donohoe R J and Swanson B I 1990 *Synth. Met.* at press
[24] Arrington C T private communication